J|A|C|S
ARTICLES
Published on Web 04/04/2003

Exfoliated Nanosheets as a New Strong Solid Acid Catalyst

Atsushi Takagaki,[†] Mariko Sugisawa,[†] Darling Lu,[‡] Junko N. Kondo,[†] Michikazu Hara,[†] Kazunari Domen,*[,‡] and Shigenobu Hayashi[§]

Contribution from the Chemical Resources Laboratory, Tokyo Institute of Technology, 4259 Nagatsuta, Midori-ku, Yokohama 226-8503, Japan, Core Research for Evolutional Science and Technology (CREST), Japan Science and Technology Company, 4-1-8 Honcho, Kawaguchi, Saitama, 332-0012, Japan, and Institute for Materials & Chemical Process, National Institute of Advanced Industrial Science and Technology (AIST), Central 5, 1-1-1 Higashi, Tsukuba, Ibaraki 305-8565, Japan

Received January 9, 2003; E-mail: kdomen@res.titech.ac.jp

Abstract: Two-dimensional metal oxide sheets in $HTiNbO_5$ and $HSr_2Nb_3O_{10}$, cation-exchangeable layered metal oxides, were examined as solid acid catalysts. Exfoliation of $HTiNbO_5$ and $HSr_2Nb_3O_{10}$ in aqueous solutions formed colloidal single-crystal $TiNbO_5^-$ and $Sr_2Nb_3O_{10}^-$ nanosheets, which precipitated under an acidic condition to form aggregates of $HTiNbO_5$ nanosheets and $HSr_2Nb_3O_{10}$ nanosheets. Although esterification of acetic acid, cracking of cumene, and dehydration of 2-propanol were not catalyzed by original $HTiNbO_5$ because of the narrow interlayer distance, which prevents the insertion of organic molecules, $HTiNbO_5$ nanosheets functioned as a strong solid acid catalyst for the reactions. Nanosheets of $HSr_2Nb_3O_{10}$ exhibited no or slight catalytic activity for these reactions. NH_3 temperature-programmed desorption and ^1H magic-angle spinning nuclear magnetic resonance spectroscopy revealed that $HTiNbO_5$ nanosheets have strong Brønsted acid sites, whereas $HSr_2Nb_3O_{10}$ nanosheets do not.

Introduction

Layered compounds have attracted much attention due to a wide variety of structural and electronic properties. Cation-exchangeable transition-metal layered oxides are layered compounds with particularly interesting and variable characteristics. These materials are typically synthesized as alkaline metal-containing layered oxides, consisting of polyanion sheets of transition-metal oxides with intercalated alkaline metal cations. The negatively charged metal oxide sheets function as host structures for ion-exchange reactions of alkaline metal cations with various other cations, as well as for the intercalation of small molecules such as water.[1] Among the layered cation-exchangers, clay minerals are the most extensively studied materials. In general, the negative charge density of transition-metal layered oxides is higher than that of clay minerals, and sheets of the material often exhibit electric conductivity and photoresponses based on band gap transitions. These types of layered oxides have actually been applied as photocatalysts.[2−6]

From the viewpoint of heterogeneous catalysis, these layered materials offer several attractive features. For example, the large inner surface area is potentially applicable to various catalytic reactions if the reactant molecules can be intercalated. Another interesting property is the solid acidity, which the H^+-exchanged form of the layered compound is expected to exhibit. In the case of clay minerals, such catalytic properties have already been examined extensively.[7] However, for layered transition-metal oxides, application has yet to be examined because of the difficulty associated with the intercalation of reactant molecules. This resistance to intercalation is attributed to the higher charge density of the sheets. Exfoliation of the layered sheets may be an alternative way to overcome this disadvantage and apply the layered materials to catalytic reactions. Although clay minerals have already been widely used as exfoliated sheets for catalytic reactions, such an attempt has yet to be made for transition-metal layered oxides. The progress in soft-solution processing in the past decade has now made such an attempt possible.[8−15]

[†] Tokyo Institute of Technology.
[‡] CREST, JST.
[§] AIST.

(1) Schaak, R. E.; Mallouk, T. E. *Chem. Mater.* **2002**, *14*, 1455.
(2) (a) Domen, K.; Kudo, A.; Shinozaki, A.; Tanaka, A.; Maruya, K.; Onishi, T. *J. Chem. Soc., Chem. Commun.* **1986**, 356. (b) Kudo, A.; Sayama, K.; Tanaka, A.; Asakura, K.; Domen, K.; Maruya, K.; Onishi, T. *J. Catal.* **1989**, *120*, 337.
(3) Takata, T.; Furumi, Y.; Shinohara, K.; Tanaka, A.; Hara, M.; Kondo, J. N.; Domen, K. *Chem. Mater.* **1997**, *9*, 1063.
(4) Bhat, V.; Domen, K. In *Electron Transfer in Chemistry*; Balzani, V., Ed.; Wiley−VCH: Weinheim, 2001; Vol. 4, pp 487−540.
(5) Kim, Y. I.; Salim, S.; Huq, M. J.; Mallouk, T. E. *J. Am. Chem. Soc.* **1991**, *113*, 9561.
(6) Kim, Y. I.; Keller, S. W.; Krueger, J. S.; Yonemoto, E. H.; Saupe, G. B.; Mallouk, T. E. *J. Phys. Chem. B* **1997**, *101*, 2491.
(7) Thomas, J. M. In *Intercalation Chemistry*; Whittingham, M. S., Jacobson, A. J., Eds.; Academic Press: New York, 1982; p 55−99.
(8) Sasaki, T.; Watanabe, M.; Hashizume, H.; Yamada, H.; Nakazawa, H. *J. Am. Chem. Soc.* **1996**, *118*, 8329.
(9) Abe, R.; Shinohara, K.; Tanaka, A.; Hara, M.; Kondo, J. N.; Domen, K. *Chem. Mater.* **1997**, *9*, 2179.
(10) Abe, R.; Shinohara, K.; Tanaka, A.; Hara, M.; Kondo, J. N.; Domen, K. *Chem. Mater.* **1998**, *10*, 329.
(11) Kaschak, M.; Lean, J.; Waraksa, C.; Saupe, G.; Usami, H.; Mallouk, T. E. *J. Am. Chem. Soc.* **1999**, *121*, 3435.
(12) Saupe, G. B.; Waraksa, C. C.; Kim, H.-N.; Han, Y. J.; Kasachak, D. M.; Skinner, D. M.; Mallouk, T. E. *Chem. Mater.* **2000**, *12*, 1556.
(13) Schaak, R. E.; Mallouk, T. E. *Chem. Mater.* **2000**, *12*, 3427.
(14) Schaak, R. E.; Mallouk, T. E. *J. Chem. Soc., Chem. Commun.* **2002**, 706.
(15) Han, Y.-S.; Park, I.; Choy, J.-H. *J. Mater. Chem.* **2001**, *11*, 1277.

10.1021/ja034085q CCC: $25.00

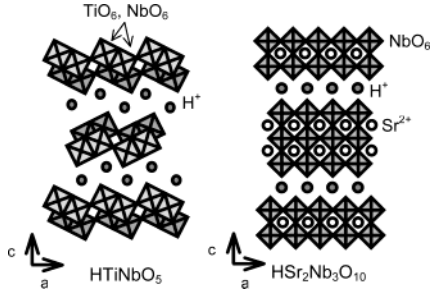

Figure 1. Schematic structures of layered $HTiNbO_5$ and $HSr_2Nb_3O_{10}$.

The exfoliated sheets are regarded as two-dimensional (2D) macropolyanions. Heteropolyanions such as $PW_{12}O_{40}^{3-}$ and $PMo_{12}O_{40}^{3-}$ are known to exhibit strong Brønsted acidity when the countercations are protons, and those materials have already been applied to several industrial catalytic processes.[16,17] The similarity of the structures of macropolyanion sheets and heteropolyanions motivated the present authors to examine the acid property of macropolyanions. A noticeable difference between the two systems is that macropolyanion sheets are heterogeneous catalysts, while heteropolyanions are essentially homogeneous ones in aqueous solutions. The development of solid acids as heterogeneous catalysts is desirable from the viewpoint of environmentally sustainable chemistry, and solid acids are in general recognized as being more environmentally benign than the corresponding homogeneous acids and liquid acids.

Another important aspect of exfoliated macropolyanion sheets is the 2D single-crystal structure. For most solid acid materials of transition-metal oxides, the surface structures are as atomically defined as in most heterogeneous catalysts. However, the exfoliated sheets maintain the 2D crystal structure, forming a precisely defined atomic structure. This facilitates examination of the origin of solid acidity based on an atomic scale and quantum chemical levels, which is not well understood for most solid acid materials. Moreover, a wide variety of cation-exchangeable transition-metal layered oxides have been reported, which will be helpful in an analysis of the strength of the solid acidity.

Following the terminology used in a recent detailed study on exfoliation by Sasaki et al., the present report will refer to exfoliated sheets as "nanosheets".[8,18−20] In this study, two typical nanosheets are chosen, $TiNbO_5^-$ and $Sr_2Nb_3O_{10}^-$, which are prepared from the relevant H^+-exchanged layered oxides, $HTiNbO_5$ and $HSr_2Nb_3O_{10}$. These nanosheets are precipitated in an acidic condition, and the resultant aggregates are examined as solid acid catalysts. The schematic structures of the aggregated precipitates of $HTiNbO_5$ nanosheets and $HSr_2Nb_3O_{10}$ nanosheets are shown in Figure 1. In $HTiNbO_5$, H^+ ions are emplaced between 2D anion sheets composed of TiO_6 and NbO_6 octahedra, while the $HSr_2Nb_3O_{10}$ is a layered perovskite consisting of perovskite layers of $Sr_2Nb_3O_{10}$ and intercalated H^+ ions.

Experimental Section

Preparation of $HTiNbO_5$ and $HSr_2Nb_3O_{10}$ Nanosheets. $HTiNbO_5$ and $HSr_2Nb_3O_{10}$ powders (5−30 μm) were prepared from $KTiNbO_5$ and $KSr_2Nb_3O_{10}$ powders according to the procedure described in the literatutre.[21,22] $TiNbO_5^-$ and $Sr_2Nb_3O_{10}^-$ nanosheets were obtained by adding 15 wt % tetra(*n*-buthylammonium)hydroxide (TBA^+OH^-) solution to 150 mL of distilled water containing 2.0 g of $HTiNbO_5$ or $HSr_2Nb_3O_{10}$.[8,11] TBA^+OH^- solution was added to the suspension until the pH reached 9.5−10.0, and the resultant solution was shaken for 3−7 days. The insertion of voluminous and hydrophilic TBA^+ cations expands and hydrates the interlayer spaces, resulting in the exfoliation of individual metal oxide sheets. The suspension was then centrifuged, and the supernatant solution containing the nanosheets was collected. Gravimetric analysis indicated concentrations of $TiNbO_5^-$ and $Sr_2Nb_3O_{10}^-$ nanosheets of 10.3 and 6.8 g L^{-1}, respectively.

The addition of a HNO_3 aqueous solution (1.0 M, 20 mL) to 30 mL of the nanosheet solution resulted in immediate aggregation of the nanosheets as a precipitate. The aggregated samples, $HTiNbO_5$ nanosheets and $HSr_2Nb_3O_{10}$ nanosheets, were rinsed 5−10 times with 100 mL of distilled water to remove HNO_3, and the complete removal of HNO_3 was confirmed by elemental analysis.

Acid Catalysis Reactions. Esterification of acetic acid, cracking of cumene, and dehydration of 2-propanol were employed as test reactions to examine the acid properties of the prepared samples. Esterification of acetic acid was examined in the liquid phase as follows: 0.20 g of the catalyst was evacuated at 453 K for 1 h and then added to a mixture of acetic acid (0.10 mol) and ethanol (0.10 mol). The reaction was carried out at 343 K in an Ar atmosphere, and the liquid phase was analyzed by gas chromatography with capillary columns. Cracking of cumene was carried out at 573 K in an atmospheric flow reaction system (catalyst, 0.20 g; cumene flow rate, 0.033 mL min^{-1}; carrier gas, N_2 (30 mL min^{-1})). The catalyst was pretreated at 573 K for 1 h under a flow of N_2 to remove water in the sample. Dehydration of 2-propanol (523 K) was also examined in the above flow reaction system (catalyst, 0.20 g; 2-propanol flow rate, 0.033 mL min^{-1}, carrier gas, N_2 (30 mL min^{-1})). In this case, the catalyst was heated at 523 K for 1 h in a flow of N_2 prior to the reaction.

For comparison, reactions using a $SiO_2-Al_2O_3$ catalyst (surface area, 685 m^2 g^{-1}) and two protonated zeolites (HZSM-5 (surface area, 326 m^2 g^{-1}) and HMOR (surface area, 205 m^2 g^{-1})) were also examined.

Characterization. The samples were characterized by X-ray diffraction (XRD; Rint 2000, Rigaku), scanning electron microscopy (SEM; S-4700, Hitachi), and transmission electron microscopy (TEM; 2010F, JEOL).

The acidity of each sample was examined using color indicator reagents and NH_3 temperature-programmed desorption (NH_3-TPD). In the color indicator experiments, the samples were evacuated at 453 K for 1 h in a Pyrex cell to remove water and then were added to a benzene solution containing the indicator reagent in a glovebox in an Ar atmosphere. NH_3-TPD was carried out using a TPD-1-AT (BEL Japan) equipped with a quadrupole mass spectrometer. After being heated at 453 K for 1 h under a He flow, 20 mg of the sample was exposed to NH_3 at 373 K for adsorption and then heated at 10 K min^{-1}.

^1H magic-angle spinning (MAS) nuclear magnetic resonance (NMR) spectra were measured at room temperature using a Bruker MSL400 spectrometer at a Larmor frequency of 400.13 MHz. A Bruker MAS probehead was used with a 4-mm zirconia rotor. The spinning rate of the sample was 8 kHz, and the ordinary single-pulse sequence was used. The frequency of the spectra was expressed with respect to neat tetramethylsilane. Experimentally, adamantane was used as a second reference material, the signal of which was set at 1.87 ppm for spinning

(16) Mizuno, N.; Misono, M. *Chem. Rev.* **1998**, *98*, 199.
(17) Okuhara, T.; Mizuno, N.; Misono, M. *Appl. Catal., A* **2001**, *222*, 63.
(18) Sasaki, T.; Watanabe, M. *J. Am. Chem. Soc.* **1998**, *120*, 4682.
(19) Sasaki, T.; Watanabe, M.; Hashizume, H.; Yamada, H.; Nakazawa, H. *J. Chem. Soc., Chem. Commun.* **1996**, 229.
(20) Sasaki, T.; Ebina, Y.; Kitami, Y.; Watanabe, M. *J. Phys. Chem. B* **2001**, *105*, 6116.
(21) Dion, M.; Ganne, M.; Tournoux, M. *Mater. Res. Bull.* **1981**, *16*, 1429.
(22) (a) Wadsley, A. D. *Acta Crystallogr.* **1964**, *17*, 623. (b) Rebbah, H.; Desgardin, G.; Raveau, B. *Mater. Res. Bull.* **1979**, *14*, 1125.

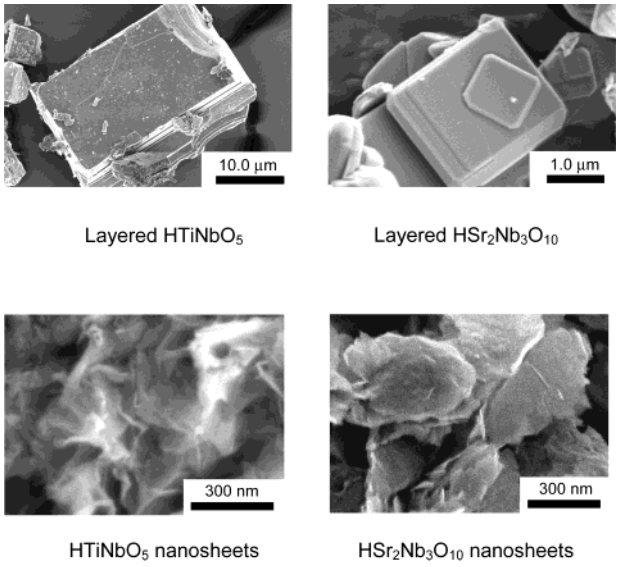

Figure 2. SEM images of layered $HTiNbO_5$ and $HSr_2Nb_3O_{10}$ and the aggregated nanosheets.

at 8 kHz. NMR spectra of dehydrated samples were measured before and after CD_3CN adsorption as follows: Dehydrated samples were obtained in a Pyrex cell in a manner similar to that above, CD_3CN vapor was introduced onto the dehydrated sample at room temperature for 30 min, and the CD_3CN-adsorbed sample was evacuated for 1 h at room temperature. The dehydrated and CD_3CN-adsorbed samples were packed into the rotor in the glovebox under a N_2 atmosphere. The seal on the rotor was good, and rehydration of the sample was not observed during NMR measurements.

Results and Discussion

1. Structures of Nanosheets and Aggregated Nanosheets. Figure 2 shows SEM images of $HTiNbO_5$, $HSr_2Nb_3O_{10}$, and the aggregated nanosheets. $HTiNbO_5$ and $HSr_2Nb_3O_{10}$ consist of tabular particles of up to 20 μm in size with a BET surface of ca. 1 $m^2\ g^{-1}$ for both samples.

TEM images and electron diffraction patterns of $TiNbO_5^-$ and $Sr_2Nb_3O_{10}^-$ nanosheets are shown in Figure 3. The clear lattice images and sharp electron diffraction patterns indicate that both nanosheets maintain the original crystal structures. It has been reported that these nanosheets are single-layer sheets.[18−20]

The SEM images of nanosheets precipitated by the addition of HNO_3 (Figure 2) indicate that the addition of H^+ randomly aggregates the nanosheets as a precipitate to form $HTiNbO_5$ and $HSr_2Nb_3O_{10}$ nanosheets with the expected compositions, as confirmed by energy-dispersive X-ray spectroscopy. Although the ideal surface areas of fully separated $HTiNbO_5$ and $HSr_2Nb_3O_{10}$ nanosheets are estimated to be 329 and 98 $m^2\ g^{-1}$ from the crystal structures, the obtained surface areas were 150 and 65 $m^2\ g^{-1}$, respectively. This indicates that certain parts (about 50% for $HTiNbO_5$ and 30% for $HSr_2Nb_3O_{10}$) of the aggregated nanosheets are not accessible by N_2, probably due to intimate contact between nanosheets.

Figure 4 shows XRD patterns for original and aggregated samples. The XRD pattern of $HTiNbO_5$ nanosheets has a weaker (002) diffraction peak and a complete absence of (004) and (008) peaks in contrast to the original sample, indicating a much poorer periodic layer structure than that of the original $HTiNbO_5$. However, diffraction peaks such as (200) and (020) corresponding to in-plane diffraction are preserved in the XRD pattern of $HTiNbO_5$ nanosheets, which means the in-plane structure is maintained after precipitation. A lack of long-range ordering of the layer structure was observed for $HSr_2Nb_3O_{10}$ nanosheets, as evidenced by the absence of (004), (006), and (0014) diffraction peaks, which are clearly observed in the original $HSr_2Nb_3O_{10}$.

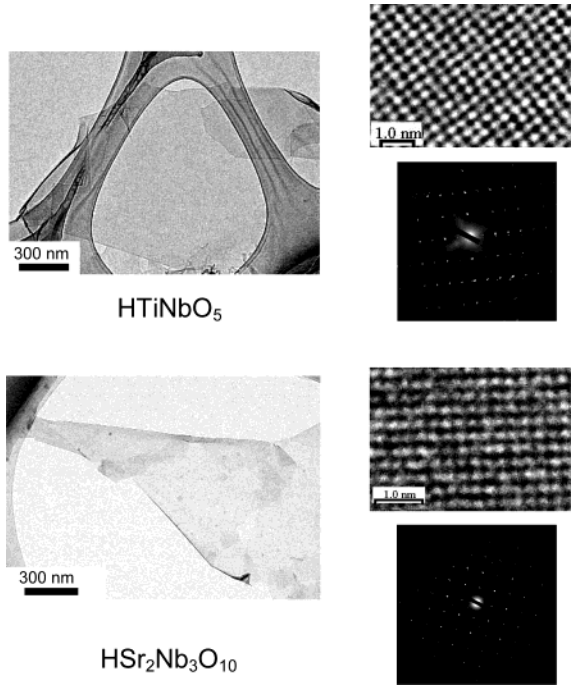

Figure 3. TEM images and electron diffraction patterns of colloidal $HTiNbO_5$ and $HSr_2Nb_3O_{10}$.

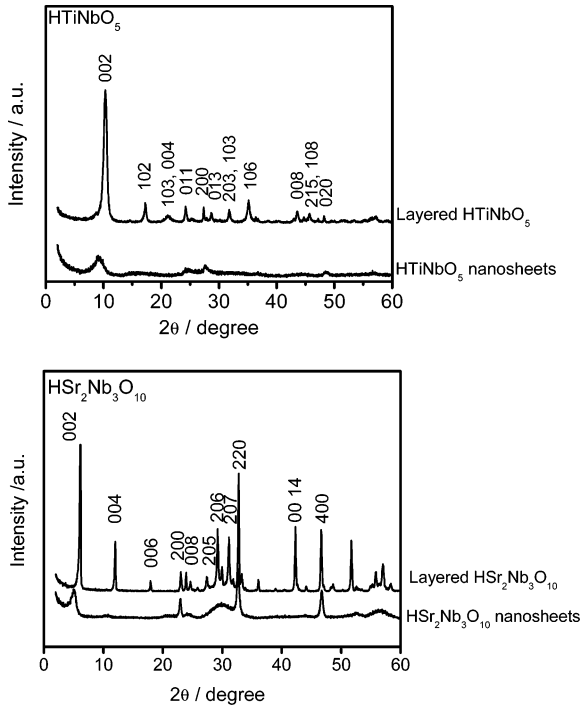

Figure 4. XRD patterns for layered and aggregated samples.

2. Acid Catalysis Reactions by $HTiNbO_5$ and $HSr_2Nb_3O_{10}$ Nanosheets. Figure 5 shows the results of ethyl acetate formation by esterification of acetic acid, cumene cracking, and dehydration of 2-propanol on $HTiNbO_5$ nanosheets and HSr_2-

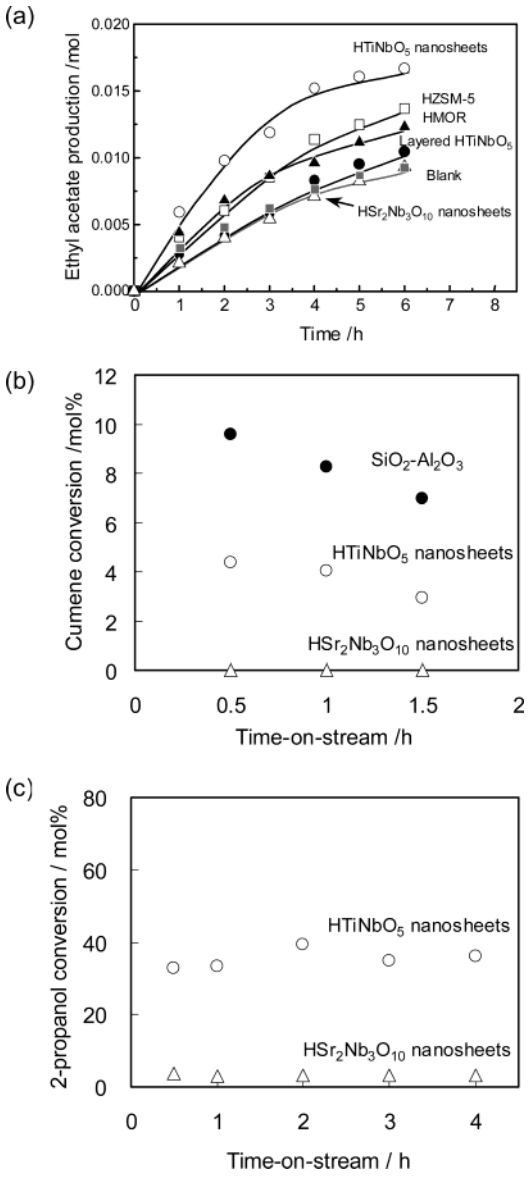

Figure 5. (a) Ethyl acetate formation on each sample at 343 K (catalyst, 0.2 g; ethanol, 0.10 mol; acetic acid, 0.10 mol). (b) Cumene conversion for each sample at 573 K (catalyst, 0.2 g; cumene flow rate, 0.033 mL min^{-1}; carrier gas, N_2). (c) 2-Propanol conversion for each sample at 523 K (catalyst, 0.2 g; 2-propanol flow rate, 0.033 mL min^{-1}; carrier gas, N_2).

Nb_3O_{10} nanosheets. It was confirmed that layered $HTiNbO_5$ and $HSr_2Nb_3O_{10}$ did not catalyze these reactions.

In the esterification of acetic acid (Figure 5a), time courses of ethyl acetate formation on layered $HTiNbO_5$ and two protonated zeolites (HZSM-5 and HMOR) were also shown for comparison. These zeolites were evacuated at 773 K for 1 h prior to reaction. Any side reactions were not observed in the reactions. Esterification of acetic acid proceeds without catalysts to some extent, as demonstrated in a blank test, because acetic acid itself catalyzes the reaction.[23] Water produced by esterification suppresses the rate of ethyl acetate formation as the reaction proceeds. The estimated amount of ethyl acetate produced at the equilibrium condition is 0.66 mol, indicating that equilibrium conditions do not suppress ethyl acetate formation. Although $HTiNbO_5$ nanosheets exhibited higher activity for the esterification of acetic acid than did the zeolites, there was no difference in the rates of ethyl acetate formation between original $HTiNbO_5$ and the blank test. This indicates that the interlayer H^+ ions in layered $HTiNbO_5$ are not available for the acid catalytic reaction because the reactant molecules are unable to penetrate into the interlayer space to utilize the H^+ ions as a catalyst. In contrast, $HSr_2Nb_3O_{10}$ nanosheets exhibited no activity for the reaction.

In the case of cumene cracking, for comparison, the reaction using a $SiO_2-Al_2O_3$ catalyst (surface area: 685 m^2 g^{-1}, 0.2 g) as a typical solid acid catalyst was examined. Cumene cracking again proceeds on $HTiNbO_5$ nanosheets, but $SiO_2-Al_2O_3$ gave higher conversion. The turnover frequencies of the effective acid sites on $HTiNbO_5$ nanosheets and $SiO_2-Al_2O_3$ after reaction for 30 min were estimated to be 5.3×10^{-4} and 5.6×10^{-4} s^{-1}, respectively,[24] suggesting that the catalytic activity of $HTiNbO_5$ nanosheets is comparable to that of the $SiO_2-Al_2O_3$. In both catalysts, any products other than benzene and propylene were not detected during reaction by gas chromatography, but cumene conversion decreased with the progress of the reaction because the catalyst surfaces became covered with carbon due to coking. $HSr_2Nb_3O_{10}$ nanosheets did not catalyze the reaction again.

To demonstrate the difference in acid catalysis between $HTiNbO_5$ and $HSr_2Nb_3O_{10}$ nanosheets, dehydration of 2-propanol by these nanosheets was also carried out in the flow reaction system (Figure 5c). The reaction proceeded on $HTiNbO_5$ nanosheets without a decrease in activity. While $HSr_2Nb_3O_{10}$ nanosheets exhibited very little activity for the reaction, the conversion was only 3%. In both cases, only propylene was formed during the reaction.

3. Acidities of $HTiNbO_5$ and $HSr_2Nb_3O_{10}$ Nanosheets. Esterification of acetic acid, cracking of cumene, and dehydration of 2-propanol revealed that $HTiNbO_5$ nanosheets act as a solid acid catalyst, whereas $HSr_2Nb_3O_{10}$ nanosheets exhibit no or slight acid catalytic activity. To clarify the difference between the acid catalysis reactions of these materials, the acidities were examined using color indicator reagents and NH_3-TPD. The coloration by each indicator reagent is summarized in Table 1. For $HTiNbO_5$ nanosheets, a yellow color developed in anthraquinone, indicating that the acidity of the sample corresponds to 90% sulfuric acid or stronger. No coloration was observed for $HSr_2Nb_3O_{10}$ nanosheets, even in chalcone.

(23) Mukai, S. R.; Masuda, T.; Ogino, I.; Hashimoto, K. *Appl. Catal., A* **1997**, *165*, 219.

(24) The amount of effective acid sites on $HTiNbO_5$ nanosheets was estimated by thermogravimetric analysis (TGA) and ^1H MAS NMR. The total amount of hydroxyl groups on 0.2 g of $HTiNbO_5$ nanosheets was estimated to be 5.7×10^{-4} mol by TGA of the nanosheets after removal of adsorbed water. In the ^1H MAS NMR spectrum for $HTiNbO_5$ nanosheets after removal of adsorbed water, four peaks due to surface hydroxyl groups were observed at 12, 7.6, 4.9, and 1.6 ppm (see below, Figures 9 and 11), and only the peak at 7.6 ppm (14% of the total amount of hydroxyl groups) among these peaks can be assigned to strong Brønsted acid sites available for the reactions (see below). Assuming that the peak at 7.6 ppm is attributed to active sites for cumene cracking, we estimated the amount of effective acid sites on 0.2 g of $HTiNbO_5$ nanosheets to be 5.7×10^{-4} mol $\times$ $0.14 = 7.9 \times 10^{-5}$ mol. In the case of the $SiO_2-Al_2O_3$ catalyst, the amount of the acid sites was obtained by transmission infrared spectroscopy of CO-adsorbed $SiO_2-Al_2O_3$ catalyst. It has been reported that the amounts of acid sites on solid acid catalysts are determined by transmission infrared spectroscopy of CO-adsorbed catalysts,[25] and the total amount of acid sites on the $SiO_2-Al_2O_3$ catalyst (0.2 g) was estimated to be 1.6×10^{-4} mol. In an infrared spectrum of $HTiNbO_5$ nanosheets, several peaks due to hydroxyl groups were observed at 3640−3680 cm^{-1}. However, these peaks were so broad that we could not obtain reliable information with respect to the amount of acid sites on $HTiNbO_5$ nanosheets by infrared spectroscopy.

Table 1. Coloration by Color Indicator Reagents for $HTiNbO_5$ Nanosheets and $HSr_2Nb_3O_{10}$ Nanosheets

indicator reagent	pK_a	coloration: $HTiNbO_5$ nanosheets	coloration: $HSr_2Nb_3O_{10}$ nanosheets
methyl yellow	+3.3	+	+
benzenazodiphenylamine	+1.2	+	+
chalcone	−5.6	+	−
anthraquinone	−8.2	+	−

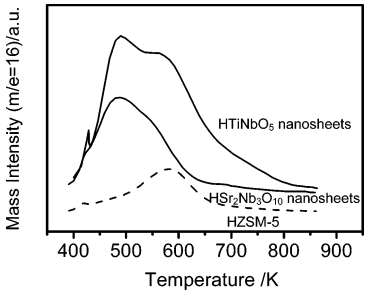

Figure 6. NH_3-TPD ($m/e = 16$) curves for aggregated $HTiNbO_5$ and $HSr_2Nb_3O_{10}$ (sample: 20 mg).

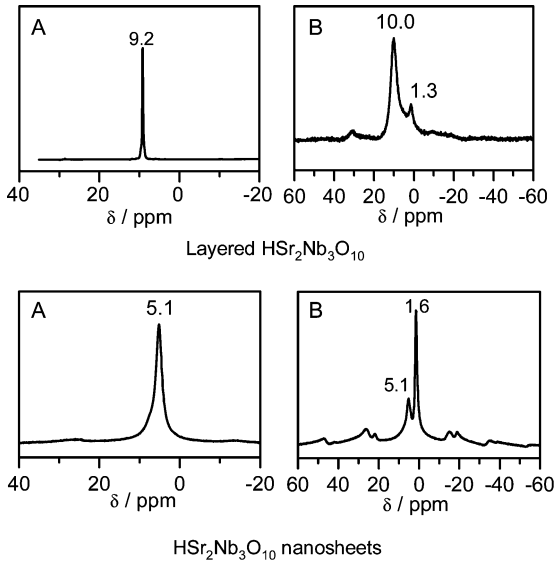

Figure 7. ^1H MAS NMR spectra for layered $HSr_2Nb_3O_{10}$ and $HSr_2Nb_3O_{10}$ nanosheets at room temperature (A) before dehydration and (B) after dehydration.

Figure 6 shows the NH_3-TPD ($m/e = 16$) results for both samples and for HZSM-5. The desorption peak for HZSM-5, a typical strong solid acid, appears at 580 K and tails to about 700 K. $HTiNbO_5$ nanosheets have a large peak at 480 K and another peak at about 580 K. It is noted that an additional peak, which is not completely separated, is observable at ca. 750 K and tails to above 800 K. These results indicate that $HTiNbO_5$ nanosheets have stronger acid sites than those of HZSM-5. For $HSr_2Nb_3O_{10}$ nanosheets, two peaks appear at 480 and 540 K, but no significant desorption occurred at higher temperatures, suggesting the complete absence of strong acid sites.

4. ^1H MAS NMR. 4.1. Layered $HSr_2Nb_3O_{10}$ and $HSr_2Nb_3O_{10}$ Nanosheets. The properties of hydrogen species at the interlayer space and on the nanosheets was examined in detail by ^1H MAS NMR spectroscopy. The ^1H chemical shift reflects the acidic property, and hydrogen species with a large chemical shift are expected to possess strong acidity.

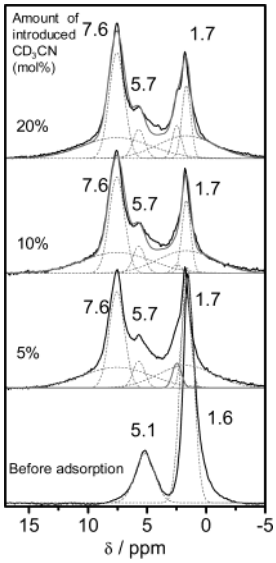

Figure 8. ^1H MAS NMR spectra for $HSr_2Nb_3O_{10}$ nanosheets before and after CD_3CN adsorption.

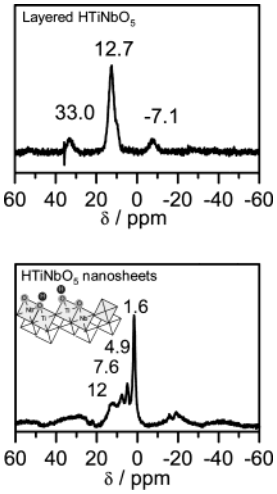

Figure 9. ^1H MAS NMR spectra for layered and $HTiNbO_5$ nanosheets after dehydration.

Figure 7 shows ^1H MAS NMR spectra (room temperature) for layered $HSr_2Nb_3O_{10}$ and $HSr_2Nb_3O_{10}$ nanosheets before and after removal of adsorbed water. A sharp peak is observed at 9.2 ppm in the spectrum for layered $HSr_2Nb_3O_{10}$ before dehydration (Figure 7A). It is known that protonated layered perovskites facilitate intercalation of water into the interlayer space.[26] The amount of intercalated water in 1 mol of layered $HSr_2Nb_3O_{10}$ was estimated to be 1.1 mol ($HSr_2Nb_3O_{10}\cdot 1.1H_2O$) by thermogravimetry. As H_3O^+ has a chemical shift of about 11 ppm,[27] and neat water has a shift of 4.877 ppm,[28] the value of 9.2 ppm is attributed to a mixture of primarily H_3O^+ with minor H_2O. Only one peak is observed for H_3O^+ and H_2O because of the fast chemical exchange between the two species. The sharp peak indicates that this species has high mobility.

(25) Wakabayashi, F.; Kondo, J. N.; Domen, K.; Hirose, C. *J. Phys. Chem.* **1995**, *99*, 10573.
(26) (a) Jacobson, A. J.; Johnson, J. W.; Lewandowski, J. T. *Inorg. Chem.* **1985**, *24*, 3727. (b) Jacobson, A. J.; Lewandowski, J. T.; Johnson, J. W. *Mater. Res. Bull.* **1990**, *25*, 679.
(27) Ratcliffe, C. I.; Ripmeester, J. A.; Tse, J. S. *Chem. Phys. Lett.* **1985**, *120*, 427.
(28) Hayashi, S.; Yanagisawa, M.; Hayamizu, K. *Anal. Sci.* **1991**, *7*, 955.

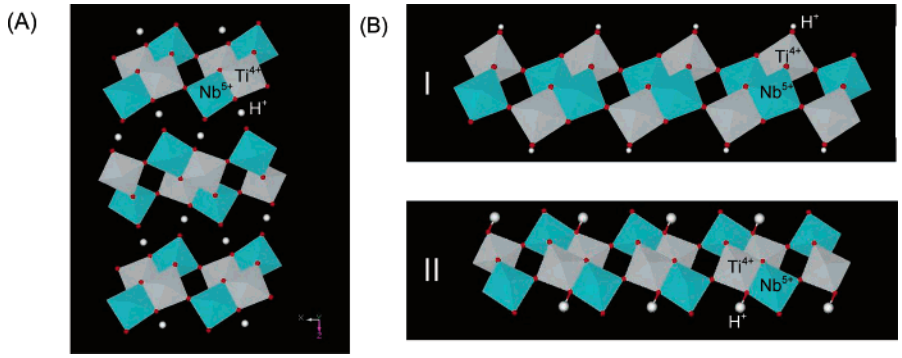

Figure 10. Schematic structures of layered $HTiNbO_5$ and $HTiNbO_5$ nanosheets: (A) layered $HTiNbO_5$ and (B) $HTiNbO_5$ nanosheets.

The interlayer water desorbs at ca. 400 K, and the dehydrated sample was obtained by heating at 423 K for 1 h. Two isotropic peaks are observed at 10.0 and 1.3 ppm for the dehydrated sample (Figure 7B). All other peaks are spinning sidebands. The peak at 10.0 ppm is due to strongly acidic OH groups fixed in the interlayer space. Strong hydrogen bonding between the layers causes the large chemical shift. A peak at 1.3 ppm is assigned to isolated OH groups without hydrogen bonds. The relatively high intensity of the spinning sidebands indicates that the dehydrated species are highly immobile.

Figure 7 also shows the NMR spectra for $HSr_2Nb_3O_{10}$ nanosheets before and after removal of adsorbed water. In the spectrum before dehydration, a single peak appears at 5.1 ppm. This peak is attributed to water, which has a chemical shift of ca. 5 ppm. The peak of OH groups on the nanosheets merges into the peak for water due to chemical exchange. After dehydration, two peaks are observed at 5.1 and 1.6 ppm. The latter is ascribed to isolated OH groups without hydrogen bonds, and the former is attributed to OH groups with hydrogen bonds, although the hydrogen bonds are weaker than those in layered $HSr_2Nb_3O_{10}$.

To further understand the behavior of the hydrogen species in $HSr_2Nb_3O_{10}$ nanosheets, CD_3CN was introduced as a probe molecule.[27] Figure 8 shows the NMR spectra of $HSr_2Nb_3O_{10}$ nanosheets with various amounts of adsorbed CD_3CN, 5, 10, and 20 mol % CD_3CN with respect to the total H amount in the $HSr_2Nb_3O_{10}$ nanosheets.

Four peaks are observed at 7.6, 5.7, 2.5, and 1.7 ppm for the sample with 5 mol % CD_3CN. With increasing adsorption of CD_3CN, the relative intensity of the 7.6 ppm peak increases, while that of the 1.7 ppm peak decreases. This change is pronounced in the sample adsorbed with 5 mol % CD_3CN. Taking account of the intensity of each peak and literature data,[29] we concluded that the peak at 5.1 ppm and part of the peak at 1.6 ppm are shifted to 7.6 and 5.7 ppm by CD_3CN adsorption. The peak at 2.5 ppm is observed as a shoulder of the peak at 1.7 ppm. It is unclear whether this peak existed before CD_3CN adsorption or was formed by CD_3CN adsorption.

Pazé et al. reported the ^1H chemical shift changes caused by CD_3CN adsorption on zeolites.[29] For H-ferrierite, the peak at 4.4 ppm due to strong Brønsted sites shifts to 11.2 ppm, and the 1.7 ppm peak of silanol shifts to 4.7 ppm. Similarly, H-β exhibits changes in peaks at 4.4 and from 3−7 ppm to 11 ppm and then to 12 ppm for strong Brønsted sites and a change from 1.8 to 5 ppm for silanol. The chemical shifts of 7.6 ppm observed in CD_3CN-adsorbed $HSr_2Nb_3O_{10}$ nanosheets are much smaller than those of the strong Brønsted sites, indicating that there are no strong acid sites on $HSr_2Nb_3O_{10}$ nanosheets.

^1H MAS NMR revealed that strongly acidic species in layered $HSr_2Nb_3O_{10}$ disappear in $HSr_2Nb_3O_{10}$ nanosheets prepared by exfoliation and aggregation. This can be attributed to the disappearance of the interlayer spaces. Strong hydrogen bonds are formed in the narrow interlayer clearance, which make the OH groups strongly acidic. Such strong hydrogen bonds disappear with the formation of $HSr_2Nb_3O_{10}$ nanosheets.

4.2. Layered $HTiNbO_5$ and $HTiNbO_5$ Nanosheets. Figure 9 shows ^1H MAS NMR spectra for layered $HTiNbO_5$ and $HTiNbO_5$ nanosheets after dehydration. The spectrum for the layered sample has a peak at 12.7 ppm with a shoulder. This chemical shift is larger than that of layered $HSr_2Nb_3O_{10}$, indicating stronger hydrogen bonds and hence stronger acidity. In the case of $HTiNbO_5$ nanosheets, four peaks are observed at 12, 7.6, 4.9, and 1.6 ppm. The peak at 12 ppm is ascribed to OH groups in an environment similar to that of layered $HTiNbO_5$, suggesting that some of the exfoliated sheets aggregate in a regular stacking pattern. Layered $HTiNbO_5$ exhibits no activity for acid catalysis reactions, indicating that the OH groups are not available for these reactions in this case.

It is essential for the assignment of the peaks at 7.6, 4.9, and 1.6 ppm to take into account the detailed structure of $[TiNbO_5]^-$ sheets. Figure 10 shows the schematic structures of layered $HTiNbO_5$ and $HTiNbO_5$ nanosheets.

There are two kinds of alternating arrangements of TiO_6 and NbO_6 octahedra in $[TiNbO_5]^-$ sheets, as shown in Figure 10B, and all sheets are expected to consist of both of these arrangements. In layered $HTiNbO_5$, H^+ is located between an oxygen atom at the vertex of a TiO_6 or NbO_6 octahedron and an oxygen atom shared by Ti^{4+} and Nb^{5+}.[30] In $[TiNbO_5]^-$ sheets obtained by the exfoliation of layered $HTiNbO_5$, negative charge is expected to be localized on TiO_6 octahedra. When TiO_6 and NbO_6 octahedra are oriented as shown in Figure 10B-I, oxygen atoms bonded to only Ti^{4+} on the sheet surface combine with H^+ to form isolated Ti−OH. In the case shown in Figure 10B-II, oxygen atoms shared by Ti^{4+} and Nb^{5+} bind to H^+, resulting in the formation of Ti(OH)Nb. As a result, by analogy of isolated Nb−OH and hydrogen-bonded Nb−OH in $HSr_2Nb_3O_{10}$ nanosheets, the peaks at 1.6 and 4.9 ppm can be assigned to isolated Ti−OH and hydrogen-bonded Ti−OH, respectively. The peak at 7.6 ppm is not observed in the ^1H MAS NMR spectrum of

(29) Pazé, C.; Zecchina, A.; Spera, S.; Spano, G.; Rivetti, F. *Phys. Chem. Chem. Phys.* **2000**, *2*, 5756.

(30) Rebbah, H.; Pannetier, J.; Raveau, B. *J. Solid State Chem.* **1982**, *41*, 57.

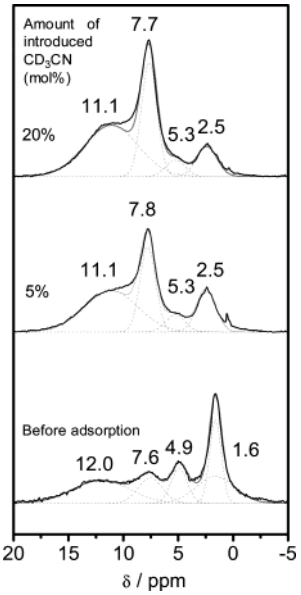

Figure 11. ^{1}H MAS NMR spectra for $HTiNbO_5$ nanosheets before and after CD_3CN adsorption.

$HSr_2Nb_3O_{10}$ nanosheets, suggesting that this peak is due to strong acid species on $HTiNbO_5$ nanosheets. It therefore seems reasonable to assign the peak at 7.6 ppm to Ti(OH)Nb.

Figure 11 shows the NMR spectra for $HTiNbO_5$ nanosheets with various amounts of adsorbed CD_3CN.

Judging from the intensity of each peak before and after CD_3CN adsorption, we found that the peaks at 4.9 and 7.6 ppm appear to shift to 7.8 and 11.1 ppm, respectively, by CD_3CN adsorption, whereas the peak at 12.0 ppm remained unchanged. The peak at 11.1 ppm overlaps the peak at 12.0 ppm, and the chemical shift of the 11.1 ppm peak observed for CD_3CN-adsorbed $HTiNbO_5$ nanosheets is comparable to that of CD_3CN-adsorbed strong Brønsted acid sites in zeolites,[29] which is consistent with the fact that $HTiNbO_5$ nanosheets function as a strong solid acid. Ti(OH)Nb presumably functions as strong Brønsted acid sites in $HTiNbO_5$ nanosheets.

Thus, Ti(OH)Nb is regarded to represent a novel strong Brønsted acid site corresponding to 90% sulfuric acid or stronger. The ^{1}H MAS NMR spectra revealed that the amount of Ti(OH)Nb on the surface of $HTiNbO_5$ nanosheets is less than 10% of the total amount of OH groups and that most of the OH groups on $HTiNbO_5$ nanosheets are in the form of isolated Ti−OH. This suggests that $HTiNbO_5$ nanosheets consist predominantly of an alternating arrangement of NbO_6 and TiO_6 octahedra similar to that shown in Figure 10B-I.

Conclusion

$HTiNbO_5$, a cation-exchangeable layered oxide, did not catalyze esterification of acetic acid, cracking of cumene, and dehydration of 2-propanol. However, $HTiNbO_5$ nanosheets functioned as a strong solid acid for these reactions due to the availability of interlayer acidic OH groups for the acid catalytic reactions. This availability follows from exposure of metal oxide sheets to liquid or gas phases. NH_3-TPD and ^{1}H MAS NMR revealed that the acid catalytic activity of $HTiNbO_5$ nanosheets is attributable to strong Brønsted acid sites, presumably Ti(OH)-Nb. In contrast, $HSr_2Nb_3O_{10}$ nanosheets exhibited no or slight acid catalytic activity for these reactions. These nanosheets host only isolated and hydrogen-bonded OH groups, which have no strong acidity.

Acknowledgment. This work was supported by the Core Research for Evolutional Science and Technology (CREST) program of the Japan Science and Technology Corporation (JST) and The 21 Century COE program from the Ministry of Education, Science, Sports, and Culture of Japan.

JA034085Q